



ARTICLE

Optical discrimination of pathological red blood cells

Michele Vergari¹  | Benedetta Niccolini² | Dario Pitocco^{2,3} | Alessandro Rizzi³ | Gabriele Ciasca^{2,3} | Marco de Spirito^{2,3} | Luca Gavioli¹ ¹Interdisciplinary Laboratories for Advanced Materials Physics (i-LAMP) and Dipartimento di Matematica e Fisica, Università Cattolica del Sacro Cuore, Brescia, Italy²Dipartimento di Neuroscienze, Sezione di Fisica, Università Cattolica del Sacro Cuore, Fondazione Policlinico Universitario "A. Gemelli", IRCCS, Rome, Italy³UOSD Diabetologia, Fondazione Policlinico Universitario Agostino Gemelli, Università Cattolica del Sacro Cuore, Rome, Italy

Correspondence

Luca Gavioli, Interdisciplinary Laboratories for Advanced Materials Physics (i-LAMP) and Dipartimento di Matematica e Fisica, Università Cattolica del Sacro Cuore, Via della Garzetta 46, 25133 Brescia, Italy.
Email: luca.gavioli@unicatt.it

Abstract

Fast diagnostic methods are crucial to reduce the burden on healthcare systems. Currently, detection of diabetes complications such as neuropathy requires time-consuming approaches to observe the correlated red blood cells (RBCs) morphological changes. To tackle this issue, an optical analysis of RBCs in air was conducted in the 250–2500 nm range. The distinct oscillations present in the scattered and direct transmittance spectra have been analyzed with both Mie theory and anomalous diffraction approximation. The results provide information about the swelling at the ends of RBCs and directly relate the optical data to RBCs morphology and deformability. Both models agree on a reduction in the size and deformability of RBCs in diabetic patients, thus opening the way to diabetes diagnosis and disease progression assessment.

KEYWORDS

anomalous diffraction approximation, erythrocyte light scattering, erythrocyte morphology, Mie theory, optical spectrum correlation with patient's health conditions, optical transmission and reflection

1 | INTRODUCTION

The physical properties of erythrocytes make the red blood cells (RBCs) key cellular indicators of the general well-being of an individual (Franco, 2012; Pretorius & Kell, 2014). The modifications of morphological and mechanical properties of RBCs, including variations in cell elasticity, rigidity, and, consequently, structural deformability and rheological properties, are associated with the pathophysiology of numerous diseases (Suresh, 2006), especially those involving inflammatory processes across various vascular systems (Pretorius & Kell, 2014; Pretorius et al., 2016). In particular, the hyperglycemia of diabetes impacts the morphology, metabolism, and function of erythrocytes (Sprague et al., 2006; Zhou et al., 2018). Mean corpuscular volume (MCV) of RBCs alone is not strongly predictive of the disease status in the case of diabetes but should be associated with its distribution (RDW) and the concentration of

HbA1c (Deccan College of Medical Sciences, India et al., 2019; Nada, 2015; Wang et al., 2021).

Since RBCs have dimensions comparable to the visible light wavelength, scattering phenomena occur and some effort has been devoted to employ light as a diagnostic tool. When a plane wave of irradiance I impinges upon an RBC the energy E subtracted from the incident beam is given by:

$$E = C_{ext} \cdot I \quad (1)$$

Where C_{ext} is the effective cross-section and can split into two parts:

$$C_{ext} = C_{scatt} + C_{abs} \quad (2)$$

C_{scatt} gives the energy dissipated by scattering and C_{abs} the energy lost due to absorption.

For RBCs in aqueous solution with a density ρ , the scattering coefficient is written as

$$\mu_s = \rho \cdot C_{scatt} \quad (3)$$

Optical measurements of μ_s or C_{scatt} (Borovoi, 1998; Faber et al., 2004; Friebe, 2010; Hammer et al., 1998; Steinke & Shepherd, 1988; Streekstra et al., 1993) have been analyzed with Mie theory (Borovoi, 1998; Hammer et al., 1998; Steinke & Shepherd, 1988), anomalous diffraction approximation (ADA) (Borovoi, 1998; Hammer et al., 1998; Streekstra et al., 1993), Fraunhofer diffraction (Streekstra et al., 1993) and Rayleigh-Gans (Hammer et al., 1998) approximation obtaining the RBC's diameter and the sphericity (Borovoi, 1998), the oxygen saturation (Faber et al., 2004) and the shear rate (Friebe et al., 2007). However, the random orientation of RBCs in solution makes it challenging to obtain accurate information on the morphology (Serebrennikova et al., 2010) and hence a direct connection with the disease. Furthermore, the C_{ext} of RBCs in aqueous solution exhibits a featureless decreasing trend as a function of increasing wavelength (except for the hemoglobin features) (Bosschaert et al., 2014; Friebe et al., 2009; Meinke et al., 2007; Roggan et al., 1999; Yaroslavsky et al., 1996), resulting in no observable oscillations in the scattered transmission in 650–1100 nm range (Meinke et al., 2005).

Here we analyze the optical behavior of RBCs deposited on a glass slide to exploit the refractive index difference between RBC and air (Park et al., 2008). The strong oscillations of the diffuse transmittance in the visible and near-infrared range are related to the RBC morphology and hence to the different health conditions through two quantitative models, based on the Mie theory and the ADA. In particular, the radius associated with the swelling on the outer region of the RBCs is consistently obtained. The results have the potential to significantly enhance the development of novel tools for early diagnosis of diabetic neuropathy, based on the detection of subtle morphological alterations in RBCs.

2 | MATERIALS AND METHODS

2.1 | Sample preparation

For this study, a total of six patients diagnosed with type 1 diabetes mellitus were recruited, comprising three patients without microvascular complications and three neuropathic patients diagnosed with diabetic sensorimotor peripheral neuropathy. A comparative analysis was performed also on a blood sample from a healthy individual and on a sample with artificially stressed RBCs in a hypertonic solution. Microvascular complications, specifically neuropathy, were diagnosed following the 2020 guidelines established by the American Diabetes Association. (American Diabetes Association, 2020) The study started after obtaining approval from the local ethics committee (protocol number: ID5860). Patients for this study were selected from the pool of patients receiving care at the

Diabetes Care Unit of the "Agostino Gemelli" University Polyclinic Foundation, IRCSS (Rome, Italy). All clinical investigations adhered to the principles outlined in the Declaration of Helsinki, with all subjects providing informed consent for their participation in the study.

Blood specimens were collected from each subject included in the study following a minimum 8-h fasting period, using vacutainers pre-coated with ethylenediaminetetraacetic acid or Heparin to prevent coagulation and stored in a refrigerator at 4°C until use. The glass slides employed for the optical measurements were covered with 1 ml of a solution of 0.01 g/L (1%) poly-L-lysine (polylysine) (from Sigma-Aldrich (USA), molecular weight range of 15,000–30,000 Da) to improve RBC adhesion. Each coated slide was left to settle at room temperature for 30 min and then rinsed three times with 1 ml of Milli-Q water. The slides were dried and stored in the refrigerator until the deposition of RBCs.

The blood samples were centrifuged for 10 min at 3000 g to separate the RBCs from the plasma following the procedure employed in a previous work (Nardini et al., 2022). For each diabetic sample, 10 μ l of the precipitate was collected and then resuspended in 1.5 ml of physiological solution (0.9% NaCl). Healthy RBC solutions were prepared at three different nominal concentrations (10 μ l, 20 μ l, and 30 μ l) in 1.5 ml of physiological solution. Additionally, the same amounts of healthy RBCs were dissolved in a hypertonic solution (2% NaCl) to induce osmotic stress in the cells.

1 ml of these solutions was combined with 0.5 ml of 1% Glutaraldehyde solution, previously filtered twice with a 0.2 μ m filter. After 30 min in the dark, the obtained solution was centrifuged for 1 min at 2000 g, the supernatant removed, and the RBCs resuspended in 1 ml of physiological solution. This procedure was repeated twice to remove any excess of Glutaraldehyde not bound to the RBCs. 1 ml of the obtained solution was deposited on the slide and left for 1 h at room temperature. Subsequently, the slides were rinsed three times with 1 ml of physiological solution to remove non-adherent RBCs, thereby forming a single layer. The RBC concentrations were chosen to ensure a density on the slide lower than a complete layer but sufficient to provide a significant optical response, thereby reducing RBC overlap.

2.2 | Data collection

The optical measurements were performed on the RBC samples deposited on the glass slides. Transmittance and reflectance spectra were measured in the range of 250–2500 nm with a data interval of 2 nm, using a Perkin-Elmer Lambda 950 spectrophotometer equipped with an integrating sphere. For each sample, we collected in air the total transmittance T_{tot} , the diffuse transmittance T_{dif} , the direct transmittance T_{dir} , the total reflectance R_{tot} , and the diffuse reflectance R_{dif} . The spectrophotometer apparatus and its configuration are discussed in detail in Section S1.

After acquiring the optical data, the samples were characterized using a Carl Zeiss AG – Supra 25 scanning electron microscope (SEM). The prepared slides were cut into 0.5 cm² samples and

attached to support stubs. Samples were covered with a gold layer (thickness ranging from 50 to 70 nm). Images of the red blood cells were captured at a magnification of 2000X with the EHT set to 6 keV. The data were analyzed using the Gwyddion software. A mask was applied to the images as shown in Figure S6 to exclude the substrate and obtain the equivalent circle radius R_{SEM} of RBCs. Random erythrocytes were selected, excluding cells in contact with the edge of the images and overlapping RBCs. The major and minor semi-axis these ellipses corresponding to RBCs were also considered through Gwyddion.

2.3 | Data analysis

The data were analyzed using Mie theory and ADA employing two different geometrical models. In the former, the determination of C_{ext} is obtained for spherical particles of radius R_g (Figure 1a) with a refractive index $\tilde{n} = n + ik$. In the latter, C_{ext} is determined assuming the scattering particle of an arbitrary shape (Figure 1b) with n close to that of the surrounding medium (in our case air, hence ADA can be used if $|\tilde{n}-1| \ll 1$). If we consider an arbitrarily shaped RBC lying in the xy plane and traversed by a plane wave propagating along the z direction as shown in Figure 1b, C_{ext} is given by:

$$C_{ext} = 2R_e \left[\iint (1 - e^{-ikd(\tilde{n}-1)}) dx dy \right] \quad (4)$$

In which R_e is the radius of the RBC, k is the wave vector and d is the path length of the light through the cell. For RBCs as shape we consider a torus that wraps around an inner disk with a thickness h . In Figure 1b a section of the modeled shape is shown. Using cylindrical coordinates and defining $r = \sqrt{x^2 + y^2}$, d is given by:

$$d(r) = \begin{cases} h & r \leq R_i \\ 2 \cdot \sqrt{R_t^2 - (r - R_e + R_t)^2} & R_i < r \leq R_e \\ 0 & r > R_e \end{cases} \quad (5)$$

with $R_i = \sqrt{R_t^2 - h^2 + R_e - R_t}$.

To directly correlate the optical spectra with the morphological features of the RBCs using the Mie theory, the optical data are fitted as described in the Section S3 using the equation:

$$C_{scatt} = N_s \cdot C_s + N_{cluster} \cdot C_{cluster} \quad (6)$$

in which C_s is the scattering cross section for isolated RBCs, N_s the number of isolated RBCs, $C_{cluster}$ the scattering cross section for aggregated and overlapped RBCs and $N_{cluster}$ the number of such clusters. The scattering cross section C_s and $C_{cluster}$ has been computed using Mie Plot. The shape of C_{scatt} is determined by C_s , while $C_{cluster}$ leads to a rigid shift as shown in Figure S4b. $C_{cluster}$ was obtained by calculating a scattering coefficient for an RBC with a radius of $3 \pm 1.5 \mu\text{m}$. Such large interval is deliberately chosen to account for the high variation in the clusters size. We used refractive index values of values of $n = 1.39$ and $\kappa = 0.01$ by averaging over literature values (Faber et al., 2004; Hammer et al., 1998; Park et al., 2008; Zhang et al., 2017) and assumed a Gaussian distribution of the RBCs radii. In this way, it is possible to determine the RBC size-dependent scattering coefficient C_s by using the radius R_g as fit parameter.

The optical data have been also analyzed using the ADA. To estimate the path length of the light through the RBC section, the expression (5) has been used. The integral over the area $dx dy$ was computed using the method of a spherical shell. Even in this case, Equation (6) was used to evaluate the total scattering cross section in such a way to include the scatter due to clustered RBCs. $C_{cluster}$ was computed using MiePlot with the same values of n and R used before. The fit was obtained varying R_t , R_e and h in a range between 100 and 2000 nm with 20 nm increments.

The parameters that minimized the squared point-by-point difference between the measured spectrum and the curve obtained using Equation (6) were considered as fit results. To reduce the number of calculations, the fit was performed only for the central region between 600 and 2000 nm, where the features associated with hemoglobin can be neglected (Kuenstner & Norris, 1994). For the same reason, fewer data points were considered, with a 10 nm interval between each value.

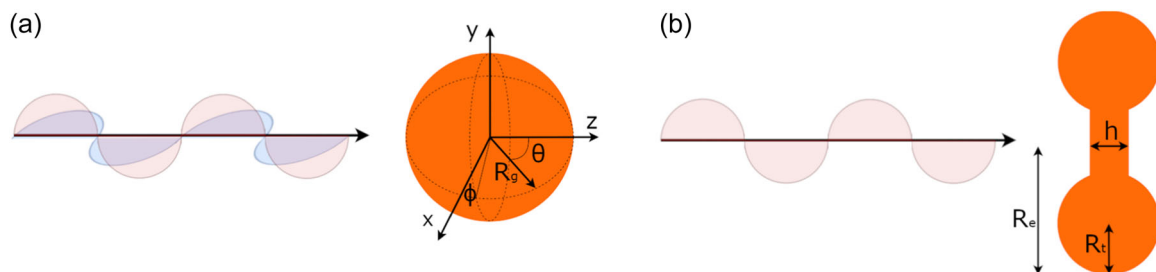


FIGURE 1 Scheme of the light-red blood cell (RBC) geometry employed in the models. (a) Definition of the variable R_g , θ , and ϕ in the spherical coordinate system used in the Mie theory. (b) Cross-sectional representation of a simplified RBC in which the inner radius R_i , the external radius R_e , the thickness h of the internal region used in the ADA are depicted. In both cases, a plane wave propagating in the positive direction of the Z -axis is considered.

3 | RESULTS AND DISCUSSION

The total transmittance and total reflectance spectra for the most morphologically different samples, the healthy one and those stressed in hypertonic solution are reported in Figure S5a, b, respectively. The data show the peaks due to the hemoglobin, but no features related to the RBCs morphology. Furthermore, the absorption spectra (Figure S5c) indicate that in the 600 and 2000 nm range, the data follows the trend of the glass coated with polylysine. Figure 2a reports the experimental diffuse transmittance of the various samples. The data significantly differ from each other in both intensity and features. A qualitative inspection of Figure 2a clearly reveals that RBCs obtained from subjects in different clinical conditions exhibit distinct spectral responses. Notably, we can discern a shift to smaller wavelengths in the oscillations position of the optical spectra in diabetic (light to dark green curves) and even more in neuropathic (light to dark orange curves) samples with respect to healthy RBCs (blue curve). For example, the first minimum of the oscillations observed at 840 nm in the healthy sample is shifted into the 720–820 nm range in the diabetic sample and in the 680–730 nm range in the neuropathic sample. The spectrum of stressed RBCs (red curve) exhibits entirely different oscillations compared to healthy RBCs. In the case of healthy RBCs, two oscillations are observed with maxima centered between 600–700 nm and 1600–1800 nm, respectively; while in the echinocyte spectrum, three distinct oscillations can be identified, with peaks located between 700–800 nm, 1100–1200 nm, and one near 2500 nm. We can also observe from Figure 2a that the first oscillation (the one observed before 800 nm) for diabetic RBCs is very pronounced, while in the healthy RBCs it is barely visible. Figure 2b shows the direct transmittance of the same samples, which present the complementary structures of Figure 2a.

This behavior in air has not been observed previously in literature and, ruling out thin film interference effects since the oscillations are absent in the total transmission spectra (see Figure S5a), we rationalize

these features by taking into account the scattering phenomena related to the RBC morphology, as described in detail below.

To assess the models used for discriminating the pathological RBCs, we first analyzed the spectra taken from two extreme cases, a healthy and an artificially stressed RBC. Figure 3a shows the fit (black curve) of the T_{dif} spectrum obtained for the sample containing echinocytes (red curve) using the Mie theory. There is an excellent agreement between the experimental data and the fit, except for the region before 600 nm and beyond 2000 nm, where the hemoglobin peaks are present. Indeed, the fit purposely does not account for the hemoglobin, focusing on the geometrical part of C_{ext} . The radius obtained from the fitting is $R_g = 2.52 \pm 0.18 \mu\text{m}$ and closely matches the experimental value $R_{\text{SEM}} = 2.55 \pm 0.24 \mu\text{m}$ measured through SEM. This agreement is favored by the almost spherical shape of stressed RBCs (see Figure 3b). In the case of healthy RBCs, the morphological situation is quite different. AFM (O'Reilly et al., 2001) studies indicate that RBCs deposited on a glass surface undergo a strong collapse of the central part (see also Figure 3c), which results in a toroidally shaped outer part of the cell. Figure 3a shows that also in this case there is a good agreement of the optical data (blue curve) with the fit (purple curve) and the discrepancies are again related to the hemoglobin peaks. The radius obtained by the Mie theory, $R_t = 1.33 \pm 0.31 \mu\text{m}$, is consistent with the radius of the section of the toroidal swelling (see Figure 1b). The variability range ($\pm 0.31 \mu\text{m}$) reflects the high variability in RBCs height, likely related to their deformability.

The same analysis was applied to the data acquired on diseased RBCs and is summarized in Figure 4. The data for diabetic RBCs are reported with the Mie theory and the ADA fitting in Figures 4a, b, respectively, while the data for neuropathic RBCs are reported with the Mie theory and the ADA fitting in Figures 4c, d, respectively. All the fits correspond quite well to the experimental data, although Mie works better below 1000 nm and ADA works better for wavelengths above 1500 nm. This is because the intensity of the first oscillation is damped when the RBC sizes exhibit high variability. The code used to

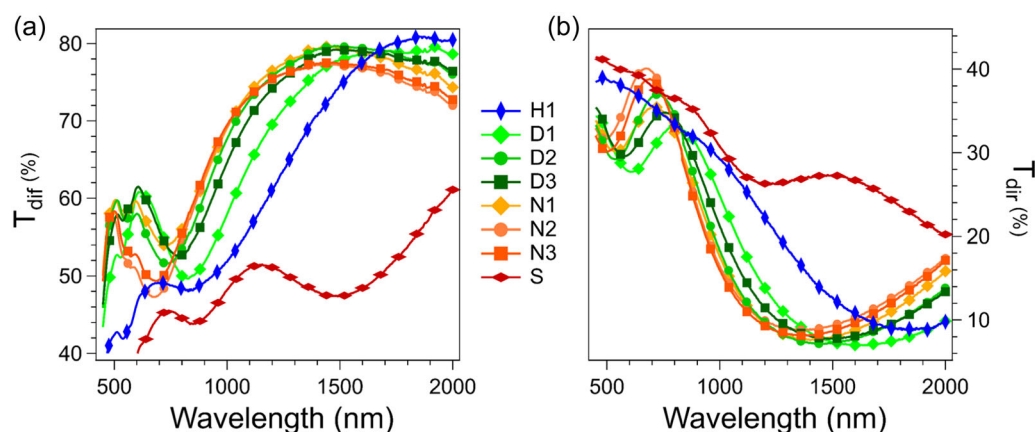


FIGURE 2 Optical transmission spectra of the different samples. Diffuse (a) and direct (b) transmittance in the 450–2000 nm range of samples with different RBC conditions: healthy (H1, blue curve), stressed (S, dark red curve) in a 2.2% NaCl hypertonic solution, diabetic (D1, D2, and D3, light to dark green curves) and neuropathic (N1, N2, and N3, light to dark orange curves). The spectra clearly show different oscillations. For the sake of clarity, the data points collected every two nm are highlighted by symbols at intervals of 80 nm.

FIGURE 3 Fitting of the data considering red blood cell (RBC) scattering for two extreme cases. (a) Diffuse transmittance in the range between 250 and 2500 nm for stressed (red curve) and healthy (blue curve) RBCs. The corresponding black and purple fit to determine C_{scatt} using Mie theory for spherical particles match well the experimental data of stressed and healthy RBCs, respectively, for wavelengths above 600 nm where the hemoglobin features. (b) and (c) SEM images of stressed and healthy RBC, respectively.

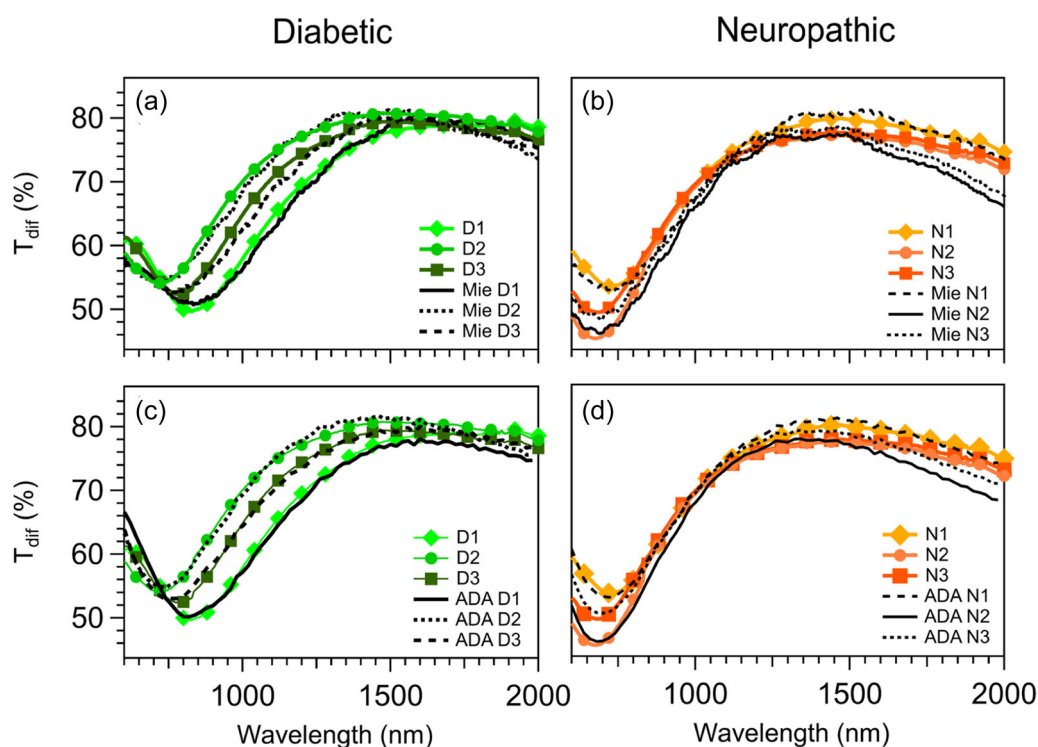
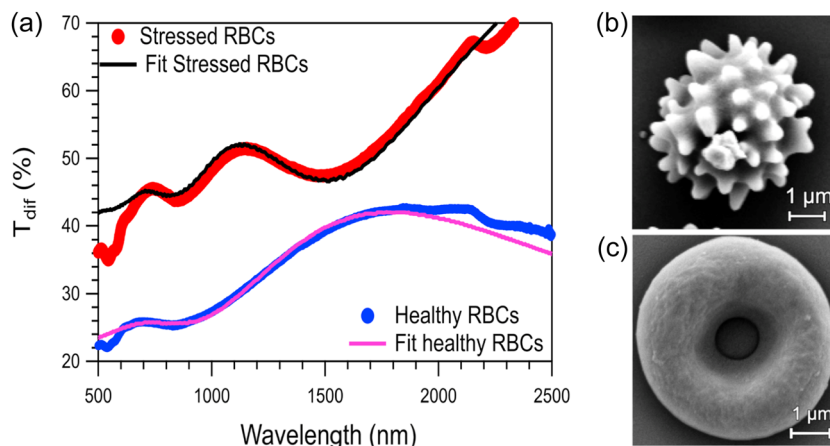


FIGURE 4 Application of the models to pathological red blood cells (RBCs) optical signals. Fit (Mie theory) of the diffuse transmittance in the range between 600 and 2000 nm for a) the diabetic samples and b) the neuropathic samples, respectively. Fit (anomalous diffraction approximation [ADA]) of the diffuse transmittance for c) the diabetic samples and d) the neuropathic samples, respectively. All samples were deposited on a glass slide with a concentration of 10 μ l of RBCs in 1.5 ml of physiological solution.

calculate C_s with ADA does not account for the width of the radius distribution, while this is considered in the Mie code. The obtained radii for all the analyzed samples, specifically R_g using the Mie theory and radii R_t of the torus in the ADA, are reported in Table 1, suggesting that, as the pathological conditions worsen, there is a reduction in the RBC radius for both methods. In general, the value of R_g is approximately 10% greater than the value of R_t , which is consistent with the fact that the Mie theory within the volume of the sphere used to approximate the cell also considers the volume of the internal area of the cell.

From the optical data, particularly from the oscillations present in the scattered transmittance, it is therefore possible to extract quantitative information on the morphology of RBCs. The employed models provide consistent results, although the ADA would require a refractive index close to 1. This requirement is not strictly verified in the current experimental conditions ($n = 1.39$) but studies on the ADA validity demonstrated that, when the size parameter $X = 2\pi R_g/\lambda$ is ranging between 3 and 12 (as in our case), the discrepancy in C_{ext} between the Mie theory and ADA for $n = 1.39$ is typically less than 20% (Liu, 1998; Videen & Chýlek, 1998). Furthermore, several studies

TABLE 1 Radii of sphere R_g using the Mie theory and radii R_t associated with the torus in the anomalous diffraction approximation (ADA) used to determine C_s for the different samples analyzed.

Samples	R_g (μm)	$\delta(\%)$	R_t (μm)	$\delta(\%)$	R_e (μm)	$\delta(\%)$	R_{SEM} (μm)	$\delta(\%)$
H1	1.3 ± 0.3	23	1.20 ± 0.07	6	3.1 ± 0.3	10	3.1 ± 0.2	6
D1	1.33 ± 0.03	2	1.18 ± 0.03	3	2.6 ± 0.2	8	2.7 ± 0.2	7
D2	1.15 ± 0.02	2	1.04 ± 0.02	2	2.9 ± 0.2	7	2.9 ± 0.2	7
D3	1.24 ± 0.02	1.5	1.10 ± 0.02	2	2.8 ± 0.2	7	2.8 ± 0.2	7
N1	1.16 ± 0.01	1	1.02 ± 0.03	1	2.6 ± 0.2	8	2.8 ± 0.2	7
N2	1.10 ± 0.01	1	0.98 ± 0.02	2	2.9 ± 0.2	7	3.0 ± 0.3	7
N3	1.10 ± 0.01	1	0.98 ± 0.02	2	2.9 ± 0.2	7	2.9 ± 0.2	7

Note: All samples were deposited on a glass slide with a concentration of $10 \mu\text{l}$ of RBCs in 1.5 ml of physiological solution.

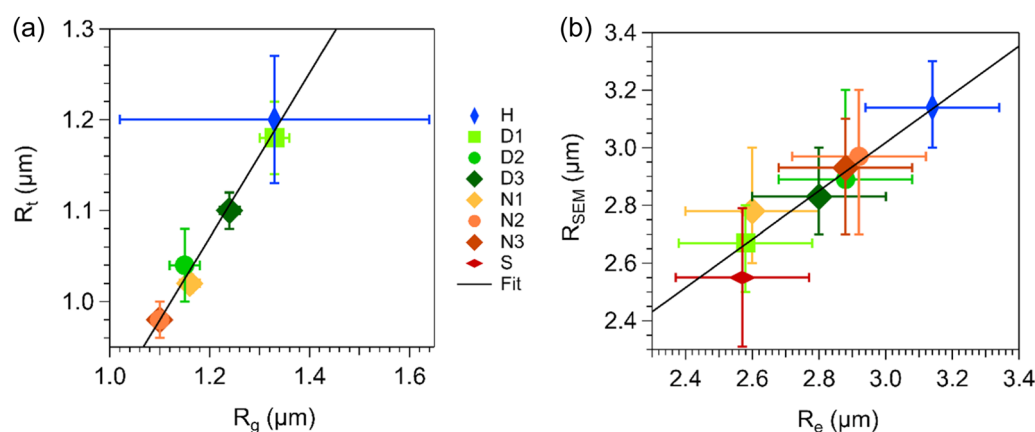


FIGURE 5 Evaluation of the morphological quantities obtained from the optical spectra. (a) Comparison between radii of sphere R_t associated to the torus in the ADA and R_g derived from Mie theory used to determine C_s for the different samples analyzed. (b) Comparison between radii R_e of RBCs on xy plane derived from ADA and the same radius R_{SEM} derived from SEM images.

have shown that ADA accurately predicts the location of the maxima and minima, which are close to the corresponding exact results calculated through the Mie theory, and that the error is primarily due to an underestimation of the oscillation amplitudes present in the C_{ext} (Cross & Latimer, 1970; Zhao & Hu, 2003). In our case, this deviation is compensated by the fitting parameter N_s . Since the multiple scattering effects are negligible, the value of R_g depends exclusively on the maxima and minima position. Therefore, unlike N_s , R_g is not affected by the limitations of the ADA.

Figure 5a shows a good linear correlation between the radii determined with the two theories with a correlation coefficient ($R^2 = 0.98$). Moreover, it can be observed from Figure 5a that neuropathic patients (orange points) tend to cluster in the bottom-left region, indicating lower values of R_t or R_g . Therefore, it is in principle possible to discriminate between diabetic and neuropathic patients using this method. Furthermore, in Figure 5b the ADA radii R_e on the xy plane (see Figure 1b) are plotted as a function of the SEM radii R_{SEM} . Also in this case there is a linear correlation ($R^2 = 0.86$) with an angular coefficient of $m = 0.8 \pm 0.3$, indicating an almost equivalent correspondence between R_e and R_{SEM} . Within this model, the disease related radii are mixed throughout the interval

thus not allowing for the discrimination between neuropathic and diabetic patients based on xy dimensions of the cell.

Both models strongly suggest a reduction in the RBC's thickness in diabetic and even more in neuropathic samples compared to controls, highlighted by the reduction of the value of R_g or R_t reported in Table 1 and Figure 5a.

In Table 2, we provide a comparison of R_g and R_t values between the two groups using a Student's t -test (despite the extremely reduced sample size). The data are reported in terms of mean and standard deviation, and p -values are shown for both one-tailed and two-tailed tests. To better discuss the diagnostic potential of the investigated optical markers, we present in the table the same analysis for RBC-associated corpuscular indices measured on the same blood tests, namely the RBC count, mean corpuscular volume (MCV), and mean corpuscular hemoglobin concentration (MCHC). Additionally, we include glycated hemoglobin levels (HbA1c), which is one of the main risk factors for the development of micro and macrovascular complications of diabetes.

Notably, the optical parameters exhibit meaningful results in one-tailed tests and are strongly suggestive of the presence of significant differences in two-tailed outcomes, despite the extremely

TABLE 2 Comparison of R_g and R_t , and red blood cell (RBC) corpuscular indices between pathological and control groups, assessed through a Student's t -test.

Variable	CTRL		Neuropathy		p-value (two-tailed)	p-value (one-tailed)
	Mean	SD	Mean	SD		
R_g (μm)	1.24	0.09	1.12	0.02	0.097	0.049
R_t (μm)	1.11	0.07	0.993	0.013	0.056	0.028
RBC count $\times 10^{12}/\text{L}$	5.0	0.2	4.6	0.54	0.363	0.182
MCV (fl)	87	4.5	86	6	0.743	0.371
MCHC (pg)	33.3	1.6	35.2	0.64	0.130	0.935
HbA1c (mmol/mol)	58	12.3	51.0	4.4	0.193	0.386

Note: The values have been approximated to maintain reasonable significant digits.

Abbreviation: SD, standard deviation.

reduced sample size. Specifically, the R_t value seems to display statistically more pronounced differences, suggesting the possibility of an improved classification performance in a clinical setting. Interestingly, the corresponding clinical RBC indices do not show or suggest the presence of statistically significant differences. This holds even for MCV, which, like R_g and R_t , indicates cell size. The potential enhanced sensitivity of the optical parameters compared to the clinical ones is likely associated with size-induced interference changes. The same sensitivity clearly cannot be achieved through the calculation of MCV. In perspective, it is important to emphasize that the results presented in Table 1 should be considered as preliminary and purely indicative. Confirmation through a dedicated study with a larger sample size is essential.

4 | CONCLUSIONS

The spectra of diffuse and direct transmittance of RBCs deposited on a glass slide exhibit various oscillations attributed to scattering phenomena. Stressed RBCs exhibit a greater number of oscillations compared to healthy RBCs, while there is a shift towards lower wavelengths in the oscillations of diabetic RBCs. Employing the Mie theory and the ADA, the dimensions of the swelling present at the ends of RBCs are obtained. Both models indicate that, as medical conditions worsen, there is a flattening of RBCs and a decrease in their deformability. Hence a direct correlation of the optical spectrum with the patient's health condition is established and this method is promising for the diagnosis of diabetes and the progression of this disease.

AUTHOR CONTRIBUTIONS

Conception and design of the work: Gabriele Ciasca, Marco de Spirito, Luca Gavioli. Experimental work: Michele Vergari, Benedetta Niccolini. Data interpretation and analysis: Michele Vergari, Gabriele Ciasca, Marco de Spirito, Luca Gavioli. Manuscript preparation including writing, critical revision and/or ultimate approval of the drafted manuscript for submission: all authors.

ACKNOWLEDGMENTS

Luca Gavioli thanks Daniela Orioni for continuous support.

DATA AVAILABILITY STATEMENT

The data that support the findings of this study are available from the corresponding author upon reasonable request. Data underlying the results presented in this paper are not publicly available at this time but may be obtained from the authors upon reasonable request.

ORCID

Michele Vergari  <https://orcid.org/0000-0001-7465-1445>

Luca Gavioli  <http://orcid.org/0000-0003-2782-7414>

REFERENCES

- American Diabetes Association. (2020). 2. Classification and diagnosis of diabetes: Standards of Medical Care in Diabetes—2020. *Diabetes Care*, 43(Suppl. ment_1), S14–S31. <https://doi.org/10.2337/dc20-S002>
- Borovoi, A. G. (1998). Scattering of light by a red blood cell. *Journal of Biomedical Optics*, 3(3), 364. <https://doi.org/10.1117/1.429883>
- Bosschaart, N., Edelman, G. J., Aalders, M. C. G., Van Leeuwen, T. G., & Faber, D. J. (2014). A literature review and novel theoretical approach on the optical properties of whole blood. *Lasers in Medical Science*, 29(2), 453–479. <https://doi.org/10.1007/s10103-013-1446-7>
- Cross, D. A., & Latimer, P. (1970). General solutions for the extinction and absorption efficiencies of arbitrarily oriented cylinders by anomalous-diffraction methods*. *Journal of the Optical Society of America*, 60(7), 904. <https://doi.org/10.1364/JOSA.60.000904>
- Faber, D. J., Aalders, M. C. G., Mik, E. G., Hooper, B. A., Van Gemert, M. J. C., & Van Leeuwen, T. G. (2004). Oxygen saturation-dependent absorption and scattering of blood. *Physical Review Letters*, 93(2), 028102. <https://doi.org/10.1103/PhysRevLett.93.028102>
- Farooqui, R., Afsar, N., & Afroze, I. A. (2019). Role and significance of hematological parameters in diabetes mellitus. *Annals of Pathology and Laboratory Medicine*, 6(3), A158–A162. <https://doi.org/10.21276/apalm.2355>
- Franco, R. S. (2012). Measurement of red cell lifespan and aging. *Transfusion Medicine and Hemotherapy*, 39(5), 302–307. <https://doi.org/10.1159/000342232>
- Friebel, M. (2010). Influence of osmolarity on the optical properties of human erythrocytes. *Journal of Biomedical Optics*, 15(5), 055005. <https://doi.org/10.1117/1.3486542>

- Friebel, M., Helfmann, J., Müller, G., & Meinke, M. (2007). Influence of shear rate on the optical properties of human blood in the spectral range 250 to 1100 nm. *Journal of Biomedical Optics*, 12(5), 054005. <https://doi.org/10.1117/1.2799154>
- Friebel, M., Helfmann, J., Netz, U., & Meinke, M. (2009). Influence of oxygen saturation on the optical scattering properties of human red blood cells in the spectral range 250 to 2000 nm. *Journal of Biomedical Optics*, 14(3), 034001. <https://doi.org/10.1117/1.3127200>
- Hammer, M., Schweitzer, D., Michel, B., Thamm, E., & Kolb, A. (1998). Single scattering by red blood cells. *Applied Optics*, 37(31), 7410. <https://doi.org/10.1364/AO.37.007410>
- Kuenstner, J. T., & Norris, K. H. (1994). Spectrophotometry of human hemoglobin in the near infrared region from 1000 to 2500 nm. *Journal of Near Infrared Spectroscopy*, 2(2), 59–65. <https://doi.org/10.1255/jnirs.32>
- Liu, C.-L. (1998). Validity of anomalous diffraction approximation in m y x domain.
- Meinke, M., Gersonde, I., Friebel, M., Helfmann, J., & Müller, G. (2005). Chemometric determination of blood parameters using visible–Near-Infrared spectra. *Applied Spectroscopy*, 59(6), 826–835. <https://doi.org/10.1366/0003702054280603>
- Meinke, M., Müller, G., Helfmann, J., & Friebel, M. (2007). Empirical model functions to calculate hematocrit-dependent optical properties of human blood. *Applied Optics*, 46(10), 1742. <https://doi.org/10.1364/AO.46.001742>
- Nada, A. M. (2015). Red cell distribution width in type 2 diabetic patients. *Diabetes, Metabolic Syndrome and Obesity: Targets and Therapy*, 8, 525–533. <https://doi.org/10.2147/DMSO.S85318>
- Nardini, M., Ciasca, G., Lauria, A., Rossi, C., Di Giacinto, F., Romanò, S., Di Santo, R., Papi, M., Palmieri, V., Perini, G., Basile, U., Alcaro, F. D., Di Stasio, E., Bizzarro, A., Masullo, C., & De Spirito, M. (2022). Sensing red blood cell nano-mechanics: Toward a novel blood biomarker for Alzheimer's disease. *Frontiers in Aging Neuroscience*, 14, 932354. <https://doi.org/10.3389/fnagi.2022.932354>
- O'Reilly, M., McDonnell, L., & O'Mullane, J. (2001). Quantification of red blood cells using atomic force microscopy. *Ultramicroscopy*, 86(1–2), 107–112. [https://doi.org/10.1016/S0304-3991\(00\)00081-4](https://doi.org/10.1016/S0304-3991(00)00081-4)
- Park, Y., Diez-Silva, M., Popescu, G., Lykotrafitis, G., Choi, W., Feld, M. S., & Suresh, S. (2008). Refractive index maps and membrane dynamics of human red blood cells parasitized by *Plasmodium falciparum*. *Proceedings of the National Academy of Sciences*, 105(37), 13730–13735. <https://doi.org/10.1073/pnas.0806100105>
- Pretorius, E., & Kell, D. B. (2014). Diagnostic morphology: Biophysical indicators for iron-driven inflammatory diseases. *Integrative Biology*, 6(5), 486–510. <https://doi.org/10.1039/C4IB00025K>
- Pretorius, E., Olumuyiwa-Akeredolu, O. O., Mbotwe, S., & Bester, J. (2016). Erythrocytes and their role as health indicator: Using structure in a patient-orientated precision medicine approach. *Blood Reviews*, 30(4), 263–274. <https://doi.org/10.1016/j.blre.2016.01.001>
- Roggan, A., Friebel, M., Dörschel, K., Hahn, A., & Müller, G. (1999). Optical properties of circulating human blood in the wavelength range 400–2500 nm. *Journal of Biomedical Optics*, 4(1), 36. <https://doi.org/10.1117/1.429919>
- Serebrennikova, Y. M., Patel, J., Milhous, W. K., & García-Rubio, L. H. (2010). Quantitative analysis of morphological alterations in *Plasmodium falciparum* infected red blood cells through theoretical interpretation of spectral measurements. *Journal of Theoretical Biology*, 265(4), 493–500. <https://doi.org/10.1016/j.jtbi.2010.05.037>
- Sprague, R. S., Stephenson, A. H., Bowles, E. A., Stumpf, M. S., & Lonigro, A. J. (2006). Reduced expression of Gi in erythrocytes of humans with type 2 diabetes is associated with impairment of both cAMP generation and ATP release. *Diabetes*, 55(12), 3588–3593. <https://doi.org/10.2337/db06-0555>
- Steinke, J. M., & Shepherd, A. P. (1988). Comparison of Mie theory and the light scattering of red blood cells. *Applied Optics*, 27(19), 4027. <https://doi.org/10.1364/AO.27.004027>
- Streekstra, G. J., Hoekstra, A. G., Nijhof, E.-J., & Heethaar, R. M. (1993). Light scattering by red blood cells in ektacytometry: Fraunhofer versus anomalous diffraction. *Applied Optics*, 32(13), 2266. <https://doi.org/10.1364/AO.32.002266>
- Suresh, S. (2006). Mechanical response of human red blood cells in health and disease: Some structure-property-function relationships. *Journal of Materials Research*, 21(8), 1871–1877. <https://doi.org/10.1557/jmr.2006.0260>
- Videen, G., & Chýlek, P. (1998). Anomalous diffraction approximation limits. *Atmospheric Research*, 49(1), 77–80. [https://doi.org/10.1016/S0169-8095\(98\)00069-6](https://doi.org/10.1016/S0169-8095(98)00069-6)
- Wang, H., Tang, C., Gao, Z., Huang, Y., Zhang, B., Wei, J., Zhao, L., & Tong, X. (2021). Potential role of natural plant medicine cyclocarya paliurus in the treatment of type 2 diabetes mellitus. *Journal of Diabetes Research*, 2021, 1–12. <https://doi.org/10.1155/2021/6656062>
- Yaroslavsky, A. N., Yaroslavsky, I. V., Goldbach, T., & Schwarzmaier, H.-J. (1996). Optical properties of blood in the near-infrared spectral range. In D. L. Farkas, R. C. Leif, A. V. Priezzhev, T. Asakura, & B. J. Tromberg (Eds.), 314–324. <https://doi.org/10.1117/12.239516>
- Zhang, Q., Zhong, L., Tang, P., Yuan, Y., Liu, S., Tian, J., & Lu, X. (2017). Quantitative refractive index distribution of single cell by combining phase-shifting interferometry and AFM imaging. *Scientific Reports*, 7(1), 2532. <https://doi.org/10.1038/s41598-017-02797-8>
- Zhao, J.-Q., & Hu, Y.-Q. (2003). Bridging technique for calculating the extinction efficiency of arbitrary shaped particles. *Applied Optics*, 42(24), 4937. <https://doi.org/10.1364/AO.42.004937>
- Zhou, Z., Mahdi, A., Tratsiakovich, Y., Zahorán, S., Kövamees, O., Nordin, F., Uribe Gonzalez, A. E., Alvarsson, M., Östenson, C.-G., Andersson, D. C., Hedin, U., Hermesz, E., Lundberg, J. O., Yang, J., & Pernow, J. (2018). Erythrocytes from patients with type 2 diabetes induce endothelial dysfunction via arginase I. *Journal of the American College of Cardiology*, 72(7), 769–780. <https://doi.org/10.1016/j.jacc.2018.05.052>

SUPPORTING INFORMATION

Additional supporting information can be found online in the Supporting Information section at the end of this article.

How to cite this article: Vergari, M., Niccolini, B., Pitocco, D., Rizzi, A., Ciasca, G., de Spirito, M., & Gavioli, L. (2024). Optical discrimination of pathological red blood cells. *Biotechnology and Bioengineering*, 121, 3311–3318. <https://doi.org/10.1002/bit.28798>